**Paper type:** Regular Paper
**Paper title:** “Flagged Parallel Manipulators”
**Authors:** M. Alberich-Carramiñana, F. Thomas, C. Torras
**Corresponding author:** Carme Torras (torras@iri.upc.edu)
**Abstract:**

The conditions for a parallel manipulator to be flagged can be simply expressed in terms of linear dependencies between the coordinates of its leg attachments, both on the base and on the platform. These dependencies permit to describe the manipulator singularities in terms of incidences between two flags (hence, the name “flagged”). Although these linear dependencies might look, at first glance, too restrictive, in this paper the family of flagged manipulators is shown to contain large subfamilies of six-legged and three-legged manipulators.

The main interest of flagged parallel manipulators is that their singularity loci admit a well-behaved decomposition, with a unique topology irrespective of the metrics of each particular design. In this paper, this topology is formally derived and all the cells, in the configuration space of the platform, of dimension 6 (non-singular) and dimension 5 (singular), together with their adjacencies, are worked out in detail.

**Index terms:** Parallel manipulators, kinematics singularities, manipulator design, stratification, flag manifold.

# Flagged Parallel Manipulators

Maria Alberich-Carramiñana, Federico Thomas, *Member, IEEE*, and Carme Torras

***Abstract*— The conditions for a parallel manipulator to be flagged can be simply expressed in terms of linear dependencies between the coordinates of its leg attachments, both on the base and on the platform. These dependencies permit to describe the manipulator singularities in terms of incidences between two flags (hence, the name "flagged"). Although these linear dependencies might look, at first glance, too restrictive, in this paper the family of flagged manipulators is shown to contain large subfamilies of six-legged and three-legged manipulators.**

**The main interest of flagged parallel manipulators is that their singularity loci admit a well-behaved decomposition, with a unique topology irrespective of the metrics of each particular design. In this paper, this topology is formally derived and all the cells, in the configuration space of the platform, of dimension 6 (non-singular) and dimension 5 (singular), together with their adjacencies, are worked out in detail.**

***Index Terms*— Parallel manipulators, kinematics singularities, manipulator design, stratification, flag manifold.**

## I. Introduction

PARALLEL robots have remarkable advantages over serial robots in terms of load-carrying capacity, stiffness, and accuracy. Nevertheless, the closed-loop nature of parallel robots limits the motion of the platform and creates complex kinematic singularities inside the workspace [20]. In a singular configuration the mechanism gains some degrees of freedom and becomes uncontrollable. Furthermore, the actuator forces may become very large which could result in a breakdown of the robot. Therefore, the identification of the singularity loci of parallel robots is a very important design and application issue.

Standard analytic techniques for identifying when a parallel manipulator is at a singularity lead to extremely large equations that are difficult to derive and, therefore, to analyze fully. Note that, for example, the singularity locus of a simple 3-RRR planar parallel manipulator for a constant orientation is the vanishing set of a polynomial of degree 42 [3].

From the design point of view, it is desirable to obtain the analytical expression of the singularity locus of any given parallel robot to determine the locations of singularities within the given workspace and try to avoid them. This work has been carried out for different particular parallel architectures (see, for example, [14], [8], [9], [26]). In 1998 Kim and Chung [17] obtained the analytic expression of the singularity locus of the general Gough-Stewart platform with constant orientation using the local structuration method. Later on, Mayer St-Onge and Gosselin [24] found the same result by expanding the Jacobian matrix of the mechanism with constant orientation using linear decomposition and cofactor expansion. Finally, very recently, Li et al [19] presented an analytic form of the six-dimensional singularity locus of the general Gough-Stewart platform. The method is based on the cascaded expansion of the determinant of the Jacobian matrix of the mechanism.

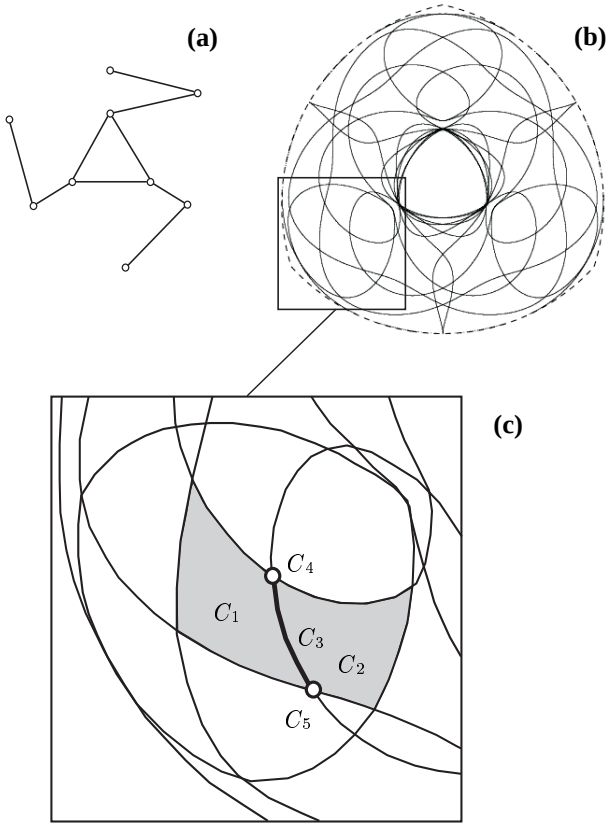


Fig. 1. The singularity locus of a 3-RRR planar parallel manipulator (a), for a constant orientation, is the root locus of a polynomial of degree 42 (b) (adapted from [3]). Then, the configuration space of the manipulator can be stratified into cells of strictly diminishing dimension (c).

The analytical expression for the singularity locus in the six-dimensional Cartesian space is a polynomial in six variables, the variables of the configuration space of the platform. Hence the singularity locus is an algebraic set embedded in the configuration space of the platform. As a consequence, this space can be decomposed into connected submanifolds of strictly-diminishing dimensions. This decomposition, together with the adjacency graph between these submanifolds, is technically known as a *stratification*. The stratification of the

The authors are with the Institut de Robòtica i Informàtica Industrial (CSIC-UPC), Llorens i Artigues 4-6, 08028-Barcelona, Spain. E-mails: maria.alberich@upc.edu, {torras, thomas}@iri.upc.edu. Maria Alberich-Carramiñana is also with the Department of Applied Mathematics I, UPC, Avda. Diagonal 647, 08028-Barcelona, Spain.

Maria Alberich-Carramiñana was supported in part by DGYCIT MTM2005-01518 and DGYCIT BFM2003-06001. Carme Torras and Federico Thomas were partially supported by the Spanish Ministry of Science and Technology (MCYT), project DPI2004-07358, and the Catalan Research Commission, through the Robotics group.

configuration space with its embedded singularity locus is much more useful for practical applications than the expression of the unstructured singularity locus itself. This can be seen through an example.

Figure 1(a) shows a 3-RRR planar parallel manipulator, whose singularity locus for a constant orientation is known to be the vanishing set of a polynomial of degree 42 [3], as displayed in Figure 1(b). The configuration space of this manipulator can be decomposed into singularity-free 2-dimensional cells, such as $C_1$ and $C_2$ in Fig. 1(c). The singularity locus defines precisely the boundaries of these 2D cells. By virtue of the decomposition being a stratification, the boundary of each 2D cell consists of singular 1D cells, as for example $C_3$, and 0D cells, as $C_4$ and $C_5$. The availability of such a well-structured description of the singularity locus permits generating trajectories away from singularities or, if required, crossing singular cells in a controlled way, so that the operative workspace of the parallel manipulator becomes enlarged.

Unfortunately, with the current tools, deriving the stratification of the singularity locus of the general Gough-Stewart platform is a fabulous task. However, this task is greatly simplified for the class of platforms known as *flagged* parallel manipulators, because the stratification of their singularity loci has been shown to have a well-behaved structure inherited from the stratification of the flag manifold [25]. Following this result, in this paper we characterize in detail the most relevant portion of the stratification of the configuration space (C-space for short) of flagged manipulators. This includes all cells of dimension 6 (non-singular) and dimension 5 (singular), together with their adjacencies. Previously to that, we assess the interest of carrying out such detailed analysis by expanding the family of flagged manipulators, which turns out to be very large.

The paper is structured as follows. Section II introduces the notion of flag and motivates the interest of flagged manipulators. In the next section the whole family of flagged manipulators is obtained in a rather intuitive way. Section IV is devoted to the stratification of the configuration space of flagged manipulators, and the topology of the cells of dimension 6 (non-singular) and dimension 5 (singular) is worked out in detail. Finally, Section V provides some conclusions and points that deserve further attention.

## II. Flags and flagged manipulators

Let us consider a plane, a line and a point so that the point is contained in the line, and the line in the plane. This geometric entity is called a flag (Fig. 2).

A parallel manipulator whose singularities can be described in terms of incidences between two flags adequately placed on its platform and base, respectively, is called a *flagged manipulator*. As an example, Figure 3 shows a 3/2 Hunt-Primrose manipulator in a singular configuration characterized by the point $v$ of the base flag lying on the line $l^*$ of the platform flag. Besides the 3/2 parallel manipulator and all its specializations, some instances of 3-2-1 manipulators are also known to be flagged [25].

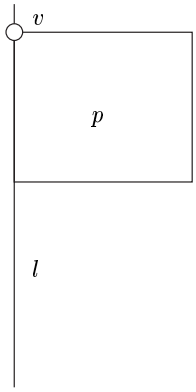


Fig. 2. A flag consists of a point, $v$, a line, $l$, and a plane, $p$, such that $v$ is on $l$ and $l$ is on $p$.

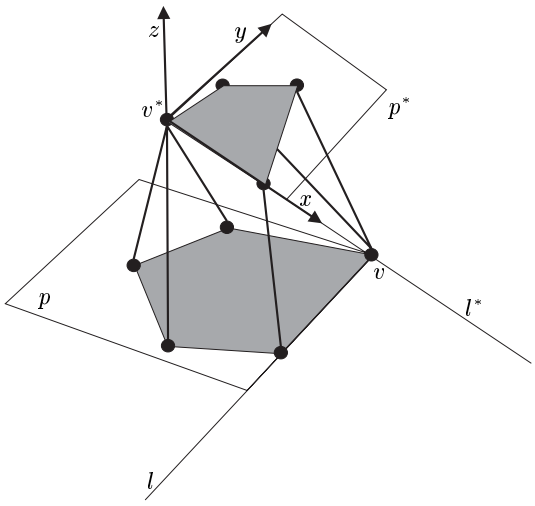


Fig. 3. A singular configuration of a 3/2 Hunt-Primrose manipulator, in which two of the tetrahedra defining its forward kinematics are degenerate.

The interest of flagged manipulators derives from the fact that their singularity analysis is quite simple, because:

1) their singularity spaces can be easily decomposed into manifolds, or cells, forming what in algebraic geometry is called a "stratification," derived from that of the flag manifold.
2) each cell can be characterized using a single local chart whose coordinates directly correspond to uncoupled translations and/or rotations in the workspace of the manipulator.

Once the nice properties of this type of manipulators were established [25], our aim in this paper is two-fold: First, we would like to assess the significance of this result by determining the size of the family of manipulators that share these properties. For this purpose, in the next section we define a transformation of the manipulator legs that leaves singularities invariant. Observe that, for all the members of the resulting family, the topology of their singularity spaces will be the same irrespective of changes in their kinematic parameters.

Second, beyond the purely combinatorial result [25], we would like to derive in detail the above-mentioned topology

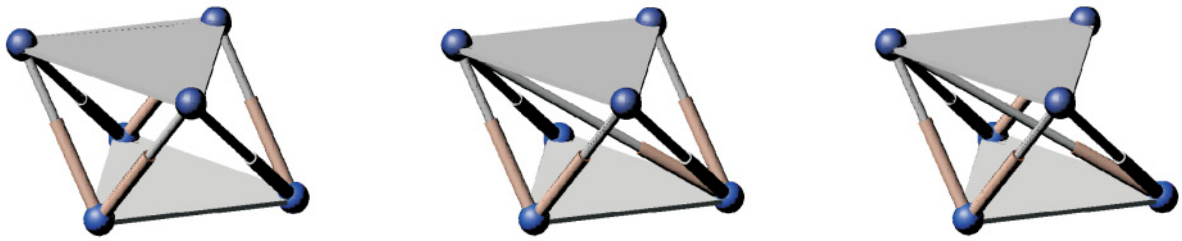

Fig. 4. The three possible architectures for the 3-3 parallel manipulators.

of singularities so that it becomes operational in practice, and it permits elucidating questions such as whether any path connecting two assembly modes passes necessarily through a singularity, a seemingly intuitive fact that not always holds [16].

## III. Expanding the Family of Flagged Manipulators

Let us consider the set of 6-legged manipulators whose leg end-points merge into three multiple spherical joints both in the base and the platform. There are only three possible architectures for this kind of manipulators, also known as 3-3 manipulators (Fig. 4). One of them corresponds to the well-known octahedral manipulator [Fig. 4(a)] whose forward kinematics is not solvable in closed-form [10]. On the contrary, the forward kinematics of the other two can be solved by a sequence of three consecutive trilaterations [15], [5], [23] leading to 8 solutions, or assembly modes.

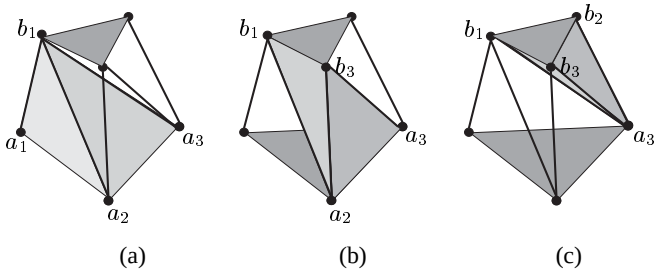


Fig. 5. The tetrahedra involved in the computation of the forward kinematics of the parallel manipulator in Fig. 4(b).

Now, let us concentrate our attention on the forward kinematics of the parallel manipulator in Fig. 4(b). Given the lengths of the segments $\overline{a_1b_1}$, $\overline{a_2b_1}$, and $\overline{a_3b_1}$, there are two possible mirror locations for $b_1$ with respect to the plane defined by $a_1$, $a_2$, and $a_3$ [Fig. 5(a)]. Once one of these two solutions for $b_1$ is chosen, $a_2$, $a_3$, $b_1$ and $b_3$ define another tetrahedron with known edge lengths [Fig. 5(b)]. Again, there are two possible mirror locations for $b_3$, in this case with respect to the plane defined by $a_2$, $a_3$, and $b_1$. Finally, after choosing one of the two solutions, $a_3$, $b_1$, $b_2$, and $b_3$ define another tetrahedron with known edge lengths [Fig. 5(c)]. In this case there are two mirror locations for $b_2$ with respect to the plane defined by $b_1$, $b_3$ and $a_3$. We conclude that if, and only if, the points in the sets $\{a_1, a_2, a_3, b_1\}$, $\{a_2, a_3, b_1, b_3\}$, and $\{a_3, b_1, b_2, b_3\}$ form non-degenerate tetrahedra, there are eight possible configurations for the moving platform compatible with a given set of leg lengths. Otherwise, the parallel manipulator is in a singularity. Alternatively, we can say that the manipulator is in a singularity if $b_1$ is on the base plane, the lines defined by $a_2a_3$ and $b_1b_3$ intersect, or $a_3$ is on the platform plane. This reinterpretation is important because it is not expressed in terms of leg locations but directly in terms of points and edges attached to either the base or the platform. Therefore, if two flags are placed on the manipulator base and platform as shown in Fig. 6, then the manipulator singularities coincide with flag configurations in which either the vertex of one flag lies on the plane of the other flag or the two flag lines intersect.

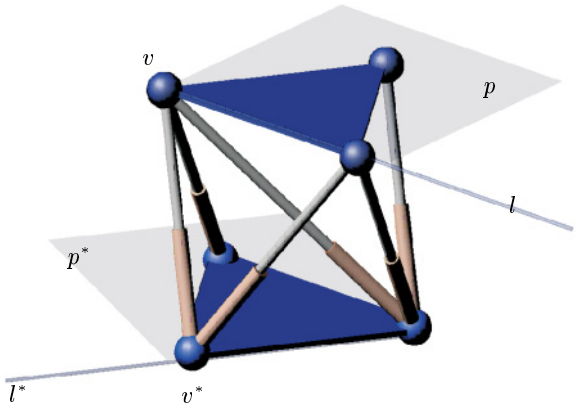


Fig. 6. The basic flagged manipulator and its attached flags.

In what follows, the parallel manipulator in Fig. 6 is called the *basic flagged manipulator*. Moreover, $v$, $l$ and $p$ will denote the point, line and plane of the flag attached to the base, while the same letters with an asterisk will stand for the same flag features of the flag attached to the platform.

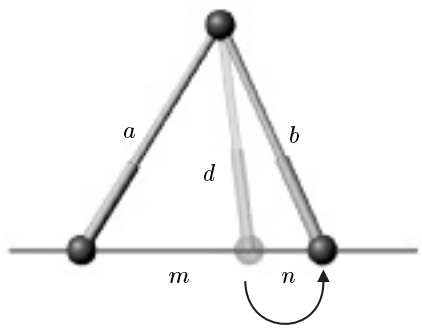


Fig. 7. Local transformation, based on Stewart's Theorem, that leaves singularities invariant.

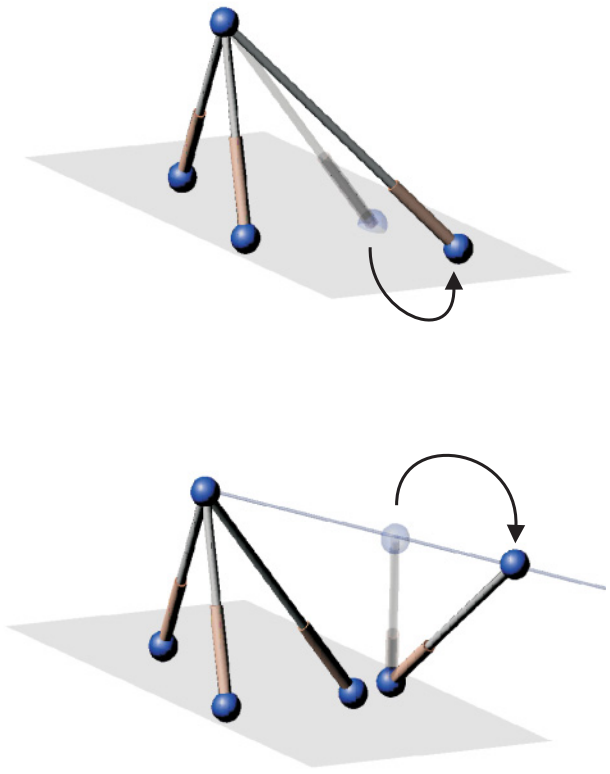

Fig. 8. Two other local transformations that can be obtained by applying twice (a) and five times (b) the transformation derived from Stewart's Theorem.

### A. The Family of 6-Legged Flagged Manipulators

It is possible to apply the local transformation shown in Fig. 7 on the location of the leg endpoints of a 6-legged manipulator with multiple spherical joints so that its singularities remain invariant. This transformation is based on a classic theorem, known as Stewart's Theorem[1], which permits finding the distance from the vertex of a triangle to any point on the line supporting the opposite side of the triangle. According to Fig. 7, the theorem states the following relationship (see [21] for more details):

$$a^2n + b^2m = (m+n)(d^2+mn) \tag{1}$$

Other local transformations can be derived from it (Fig. 8(b) and 8(c)). These transformations permit expanding the whole family of flagged manipulators shown in Fig. 9.

As an example, Fig. 10 shows how the 3/2 Hunt-Primrose manipulator [15] can be derived from the basic flagged manipulator by applying a sequence of four of these transformations.

Note that, besides the 3/2 manipulator (leftmost 4/5 instance in Fig. 9), several other members of this family have attracted attention in the past due to their nice properties. The basic 3-3 flagged manipulator was studied by Collins and McCarthy [7], who demonstrated that its singularity locus is a cubic surface that factors into three planes, which can be viewed as the flattening of the three tetrahedra appearing in Fig. 5. In Section IV-C it will become clear that these three planes or flat tetrahedra correspond to the three types of 5D cells appearing in the stratification of the singularity locus of flagged manipulators.

Zhang and Song [27] analysed a class of 6-legged manipulators that had closed-form solution, namely those that had 5 endpoints aligned in either their platform or their base. Note that all but 6 of the manipulators appearing in Fig. 9 belong to this class. Among those not belonging to the class are the already mentioned 3/2 manipulator, the (3-1-1-1)$^2$ manipulator (leftmost 4/4 instance in Fig. 9) studied by Bruyninckx [4], and the 2-1-1-2/1-1-2-1-1 manipulator (fourth on the left 4/5 instance in Fig. 9), whose potential will be discussed next.

### B. The Family of 3-Legged Flagged Parallel Manipulators

Parallel manipulators are characterized by having a base and a platform connected by serial chains. When each of these serial chains is composed of a passive universal joint, a prismatic actuator and a passive spherical joint, the resulting manipulator is called a Gough-Stewart platform. Nevertheless, more general chains can be used between the base and the platform to provide an alternative to prismatic actuators.

The just mentioned 2-1-1-2/1-1-2-1-1 manipulator (Fig. 12(a)) can be viewed as a 2-2-2 Stewart platform in which one of the 2-leg groups has been inverted, and a proper alignment of leg-endpoints on the base is maintained. The 2-leg groups can be replaced by other equivalent parallel mechanisms (Fig. 11(b)) or linear chains (Fig. 11(c)) without altering the singularity locus of the manipulator. Each substitute of a 2-leg group should be actuated either by two 1-DOF joints or by one 2-DOFs joint.

As an example, if we substitute each of the three 2-leg groups of the 2-1-1-2/1-1-2-1-1 manipulator by a PRPS serial

[1]Named after Matthew Stewart who published it in 1745.

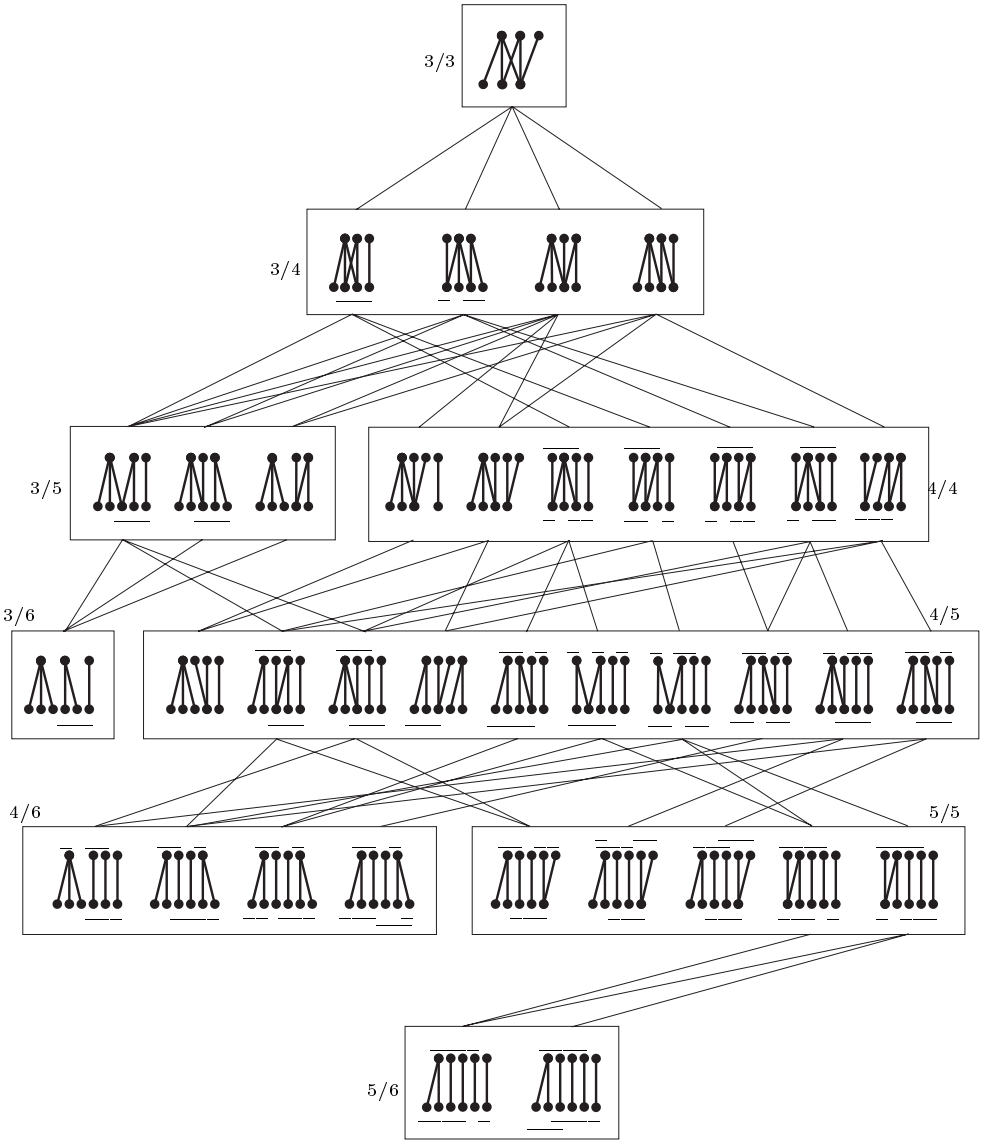


Fig. 9. The whole family of 6-legged flagged manipulators expanded from the basic one by applying the transformation in Fig. 8(a). Segments, next to either the base or the platform, indicate the endpoints that should be kept aligned.

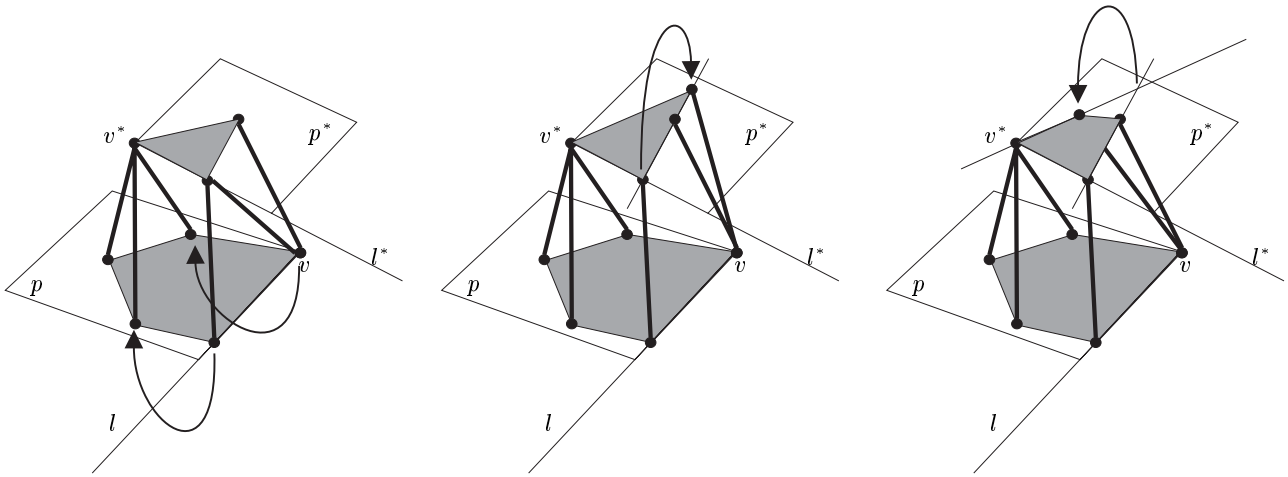


Fig. 10. The 3/2 Hunt-Primrose manipulator is a flagged manipulator because it can be obtained by applying a sequence of four local transformations to the basic flagged manipulator. Notice how the attached flags remain invariant under these transformations.

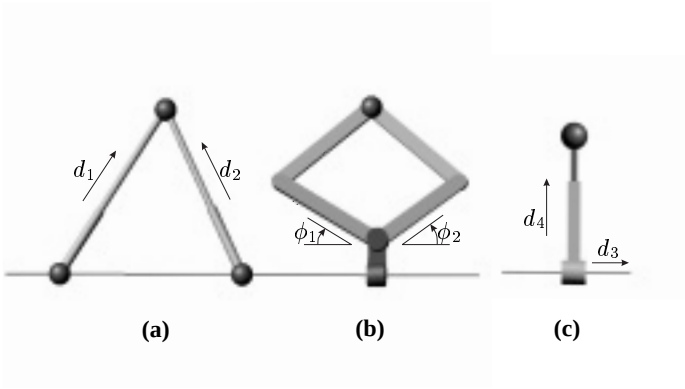


Fig. 11. **(a)** A 2-leg group can be substituted, for example, by **(b)** a pantograph, or **(c)** a PRPS serial chain.

chain (Fig. 11(c)), the result appears in Fig. 12(b). Collins and Long [6] have considered the replacement of the 2-leg groups of a 2-2-2 Stewart platform by kinematically equivalent pantograph mechanisms, such as that in Fig. 11(b).

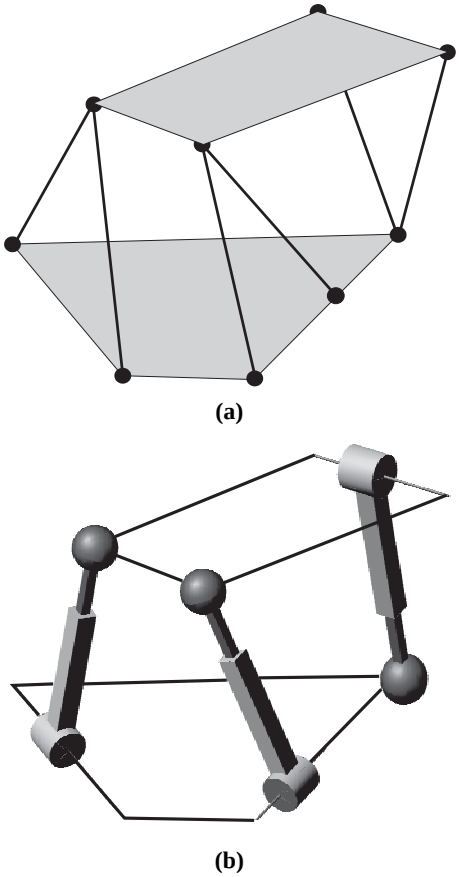


Fig. 12. **(a)** The 2-1-1-2/1-1-2-1-1 manipulator, and **(b)** a 3-legged flagged manipulator derived from it by substituting the three 2-leg groups by PRPS serial chains satisfying the required alignment on the base.

Notice that the singularities of flagged manipulators considered in this paper are those of type II in the classification of Gosselin and Angeles [12], namely those in which the platform gains one or more degrees of freedom and, therefore, cannot resist one or more forces or moments even when all actuators are locked. These are the only ones appearing when prismatic joints are taken to be unlimited. Of course, prismatic actuators have limits which originate singularities of type I, and some manipulator instances with very particular architectural parameters have singularities of type III, but these are very specific and well-studied. It is worth mentioning that, by substituting 2-leg pairs by other kinematically equivalent mechanisms, the singularities of type II remain unchanged, but new singularities of type I and type III may be introduced. For instance, the pantograph reaches a singularity of type I when the left and right chains are aligned, even for unlimited actuators. Moreover, if the four links of the pantograph have the same length, then a singularity of type III appears when the two lower links are aligned. The former corresponds to the workspace boundary, whereas the second is usually a physically unreachable configuration.

Recently, Ben-Horin and Shoham [2] have studied the replacement of the 2-leg groups of a 2-2-2 Stewart platform by kinematically equivalent serial chains involving spherical (S), prismatic (P), revolute (R), helical (H), cylindrical (C) and universal (U) joints. By substituting each of the three 2-leg groups by the same kinematic chain, they obtained 144 different manipulator architectures. If the combination of different serial chains were allowed, the number of possible manipulator architectures would grow beyond 500.000.

Likewise, the family of flagged manipulators displayed in Fig. 9 can be further expanded by replacing 2-leg groups with linear chains among the 144 identified by Ben-Horin and Shoham. Just the expansion of the 2-1-1-2/1-1-2-1-1 manipulator leads to a class as large as that developed in [2].

## IV. The topology of singularities of flagged manipulators

Once the significance of the family of flagged manipulators has been established, we will proceed to study their configuration space and, hence, their embedded singular manifolds. The *combinatorics* of the singularities of flagged manipulators was already made clear in [25], and thus here we will go on to derive the *topology* of the singularity locus in terms of the 6D and 5D cells together with their adjacencies. To this end, we should now proceed more formally.

### A. From projective flags to affine flags

*Definition 1 (Flag):* A flag in projective space $\mathbb{P}^3$ is a sequence $V_0 \subset V_1 \subset V_2 \subset \mathbb{P}^3$ of projective subspaces such that $\dim(V_i) = i$. $V_0$, $V_1$ and $V_2$ are called the *flag features*.

The Euclidean space $\mathbb{R}^3$ can be viewed as a subspace of $\mathbb{P}^3$ via $\mathbb{R}^3 \cong \mathbb{P}^3 \backslash \Pi_\infty$, where $\Pi_\infty$ stands for the plane at infinity. The flags we will be concerned with are the *affine flags*, that is, flags $V_0 \subset V_1 \subset V_2 \subset \mathbb{P}^3$ satisfying $V_0 \notin \Pi_\infty$.

In what follows, we make a slight abuse of language by identifying affine subspaces of dimensions 0, 1, and 2, in projective space $\mathbb{P}^3$ not contained in $\Pi_\infty$ with points, lines, and planes, in Euclidean space $\mathbb{R}^3$.

*Definition 2 (Flag manifold):* The flag manifold $\mathcal{F}lag(4)$ is the set of all flags in $\mathbb{P}^3$. Let $\mathcal{F}_{\mathcal{A}}(\mathbb{P}^3)$ denote the subset of the affine flags in $\mathcal{F}lag(4)$.

Let $v \subset l \subset p$ be a fixed *reference flag*. The flag manifold $\mathcal{F}lag(4)$ admits the following stratification (in fact, cell decomposition):

$$\mathcal{F}lag(4) = \cup_{w \in \sum_4} B^w, \tag{2}$$

where $B^w$ is the set of all the flags whose flag features have incidence relations with the reference flag determined by the permutation $w \in \sum_4$, with $\sum_4$ standing for the set of permutations of $4$ elements [13].

As detailed in Appendix A, each cell $B^w$ is isomorphic to $\mathbb{R}^{\text{length}(w)}$ [2] and hence it is connected. Furthermore, in the stratification (2), two cells of consecutive dimensions are adjacent if and only if there is a single transposition between their associated permutations.

This leads to an algorithmic procedure to derive the graph of cells for the flag manifold, as was displayed in [25]. Fig. 13 shows the cells of dimensions $6$ and $5$ and their adjacencies. The rectangle represents the 6D cell $B^{(4,3,2,1)}$, while the ellipses are the 5D cells: $B^{(4,3,1,2)}$, $B^{(3,4,2,1)}$ and $B^{(4,2,3,1)}$. Each 5D cell is labelled also with $v-p^*$, $p-v^*$ and $l \cdot l^*$, respectively, which characterize the incidence relations between the flag features of the flags $v^* \subset l^* \subset p^*$ in each cell and the reference flag. A hyphen between two elements denotes that one is included in the other, and a dot means that they meet at a single point.

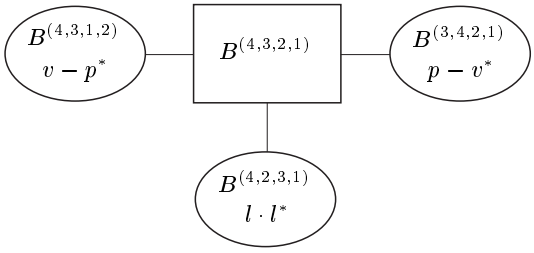


Fig. 13. Stratification of the flag manifold: the rectangle represents the 6D cell, and the ellipses are the 5D cells.

The stratification of the flag manifold $\mathcal{F}lag(4)$ induces a stratification of the subset of affine flags $\mathcal{F}_{\mathcal{A}}(\mathbb{P}^3)$. Indeed, after removing the plane at infinity $\Pi_\infty$, the resulting decomposition is still a stratification, and some cells (those whose associated permutations do not start with a 1) are split into two connected components (see Appendix B for details). Fig. 14 shows the cells of dimensions $6$ and $5$ of $\mathcal{F}_{\mathcal{A}}(\mathbb{P}^3)$ and their adjacencies. The rectangles represents the two 6D cells $B_+^{(4,3,2,1)}$ and $B_-^{(4,3,2,1)}$, while the ellipses are the six 5D cells: $B_\varepsilon^{(4,3,1,2)}$, $B_\epsilon^{(3,4,2,1)}$ and $B_\varepsilon^{(4,2,3,1)}$, with $\varepsilon \in \{+,-\}$. For the sake of clarity, each 5D cell is labelled with $(v-p^*)^\varepsilon$, $(p-v^*)^\varepsilon$ and $(l \cdot l^*)^\varepsilon$, respectively, to make explicit the incidence relations between the flag features of the flags in each cell and those of the reference flag.

The stratification of the set of affine flags induces a decomposition of the C-space of flagged manipulators, which we work out in detail in the next section.

[2]The *length* of a permutation $w$ is defined as the number of inversions in $w$, that is, $\text{length}(w) = \text{card}\{i < j : w(i) > w(j)\}$.

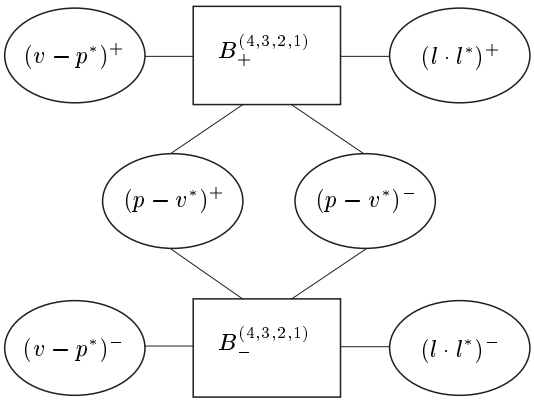


Fig. 14. Stratification of the set of affine flags: the rectangles represent the 6D cells, and the ellipses are the 5D cells.

### B. From affine flags to manipulator configurations

Given a flag $\mathcal{V}^* = (v^*, l^*, p^*)$ attached to the basic flag manipulator as in Fig. 6 (and, in general, to any other member of the family of flagged manipulators), we consider an Euclidean reference frame having $v^*$ as origin, $l^*$ as the $x$ axis, and $p^*$ as the $xy$ plane. This flag remains invariant when a rotation of $\pi$ radians about any of the three coordinate axes is applied. Formally, the group of Euclidean transformations leaving the flag invariant is $\mathcal{H}_{\mathcal{V}^*} = \{\mathbf{I}, \mathbf{R}_x, \mathbf{R}_y, \mathbf{R}_z\}$, where $\mathbf{I}$ is the identity transformation, and $\mathbf{R}_k$ stands for a rotation of $\pi$ radians about the $k$-axis. Let us mention that $\mathcal{H}_{\mathcal{V}^*}$ is one of the representations of the well-known Klein four-group, since $\mathbf{R}_x\mathbf{R}_y = \mathbf{R}_y\mathbf{R}_x = \mathbf{R}_z$, $\mathbf{R}_x\mathbf{R}_z = \mathbf{R}_z\mathbf{R}_x = \mathbf{R}_y$, and $\mathbf{R}_y\mathbf{R}_z = \mathbf{R}_z\mathbf{R}_y = \mathbf{R}_x$.

Now, let us fix an Euclidean reference frame at the base of the flagged manipulator attached to the reference flag $\mathcal{V} = (v, l, p)$ (and oriented in the same way as the frame previously fixed at the platform). Then, a manipulator configuration is described as $\mathbf{q} \in \mathbb{R}^3 \times \text{SO}(3)$, relating the platform frame to the base frame. Given one such manipulator configuration $\mathbf{q}$, we can characterize the set of 4 manipulator configurations yielding this same flag configuration as follows:

$$\left\{ \mathbf{T}\mathbf{q} \mid \mathbf{T} \in \mathcal{H}_{\mathcal{V}^*_{\mathbf{q}}} \right\}, \tag{3}$$

where $\mathcal{V}^*_{\mathbf{q}}$ is the flag associated with the platform in configuration $\mathbf{q}$. This gives a four-fold covering morphism $\pi : \mathbb{R}^3 \times \text{SO}(3) \to \mathcal{F}_{\mathcal{A}}(\mathbb{P}^3)$ sending $\mathbf{q}$ to $\mathcal{V}^*_{\mathbf{q}}$ [22]. Therefore, with each relative configuration of *two flags*, we can associate $4$ relative configurations of the platform and base.

Figure 15 shows the four platform configurations sharing the same flag $\mathcal{V}^*_{\mathbf{q}}$, namely $\mathbf{q}$, $\mathbf{R}_x\mathbf{q}$, $\mathbf{R}_y\mathbf{q}$, and $\mathbf{R}_z\mathbf{q}$.

Summarizing, the configuration space of the manipulator can be seen as a 4-fold covering of the set of affine flags. The interesting property is that it thus inherits the nice structure of the latter, as detailed in the next section.

### C. The topology of singularities

The covering morphism $\pi$ induces a stratification of $\mathbb{R}^3 \times \text{SO}(3)$, and hence of the singularity locus of the flagged manipulator, from the stratification of $\mathcal{F}_{\mathcal{A}}(\mathbb{P}^3)$ obtained in the

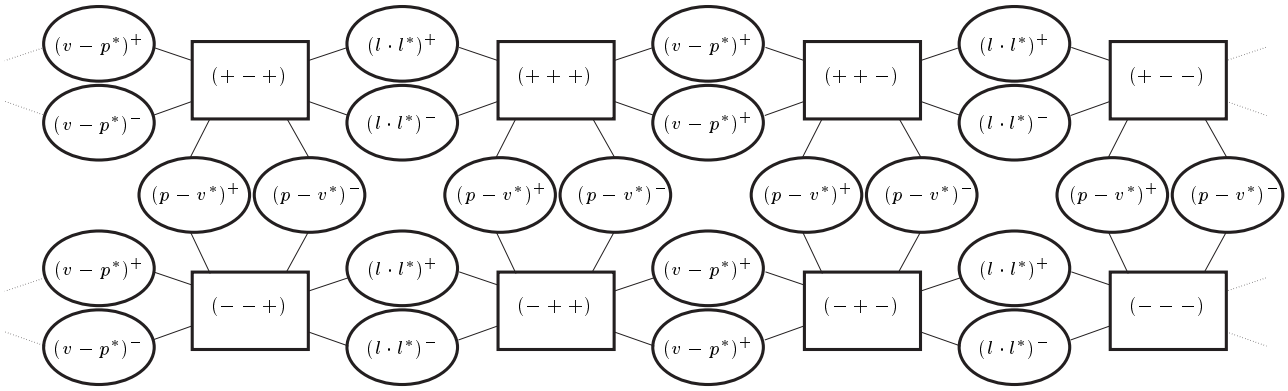


Fig. 16. The graph shows the topology of C-space for flagged manipulators. The rectangles represent the 6D cells of C-space non-singular configurations which correspond to the eight different assembly modes, while the ellipses are the 5D cells of singular configurations.

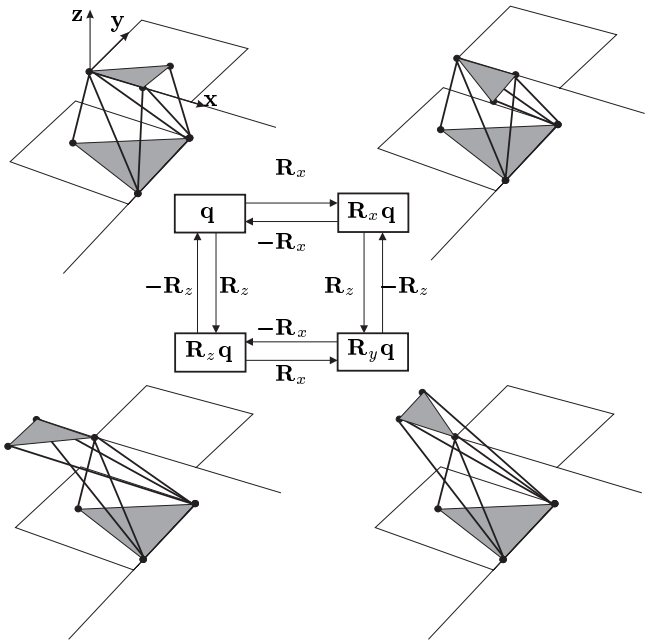


Fig. 15. The four platform configurations sharing the same flag, obtained by rotating $\pi$ radians about its reference axes.

Section IV-A. In particular, Equation (3) provides a procedure to unfold the stratification of the affine flags so as to obtain a useful decomposition of the C-space of the manipulator.

Due to the 4 degree of $\pi$, the two 6-dimensional disjoint cells in $\mathcal{F}_{\mathcal{A}}(\mathbb{P}^3)$ correspond in $\mathbb{R}^3 \times \mathrm{SO}(3)$ to 8 6D cells, that is, 8 connected components of the non-singular manipulator configurations, which (by connectness arguments) must correspond to the 8 assembly modes of the flagged manipulators. Hence there are 8 connected components of non-singular configurations in C-space. To visualize these 8 cells see Fig. 15: besides the four platform configurations sharing the same flag $\mathcal{V}^*_{\mathbf{q}}$, we could draw the other four configurations corresponding to their images by the specular reflection through the plane of the base.

Now, how are these 8 cells packed together in C-space? Owing to the placement chosen for the two flags in the manipulator, the 5D cells provide a decomposition of the singularity locus.

Recall that there are 3 5-dimensional cells in $\mathcal{F}lag(4)$, which correspond to the cases in which point $v^*$ of the platform lies on the base plane, point $v$ of the base lies on the platform plane, and lines $l$ and $l^*$ intersect. Restricted to $\mathcal{F}_{\mathcal{A}}(\mathbb{P}^3)$ they split off into 6 5-D cells. Due to the 4 degree of $\pi$, this leads in $\mathbb{R}^3 \times \mathrm{SO}(3)$ to 24 5D cells. We say that a 5D cell is *of type* $v^*-p$, $v-p^*$ or $l\cdot l^*$ if it is one of the connected components of the inverse image of a cell $(v^*-p)^\varepsilon$, $(v-p^*)^\varepsilon$ or $(l\cdot l^*)^\varepsilon$, respectively, for some $\varepsilon \in \{+,-\}$.

As detailed in Appendix C, by resorting to the theory of path lifting [18], the adjacencies between these 8 6D cells and 24 5D cells can be derived, resulting in the graph shown in Fig. 16. The rectangles represent the 8 6D connected components of C-space of non-singular configurations, while the ellipses are the 5D manifold patches of singular configurations separating these components. The 4 multiplicity appears clearly at this level as well. Note that each non-singular region has the same structure, being bounded by 6 singular regions, two of type $l\cdot l^*$, two of type $v-p^*$, and two more of type $p-v^*$. To characterize each 6D cell we can use a triple of signs corresponding to the the orientation of the three tetrahedra appearing in Fig. 5.

We are now in a suitable position to answer the question raised at the end of Section II. From the graph in Fig. 16, it is clear that any path connecting two assembly modes passes necessarily through a singularity, contrarily to what happens for other types of manipulators [16].

## V. Conclusion

The interest of flagged parallel manipulators has been established from both an intensive and an extensive viewpoint. Concerning the former, we have studied the topology of their configuration space, proving that it admits a well-behaved cell decomposition consisting of eight connected components (cells of dimension 6), corresponding to the eight possible assembly modes, separated by singularities (cells of dimension 5 and lower). The topology of these cells has been formally derived in detail, yielding a structured description of the singularity locus that permits generating trajectories that either avoid or cross singular cells in a controlled way.

To assess the importance of this class of manipulators from an extensive viewpoint, we have studied manipulator transformations that leave singularities invariant. This permits carrying out the singularity analysis on a single representative of this class and the obtained result is guaranteed to be valid for all transformed manipulators. For the sake of simplicity, the representative of the flagged parallel manipulators has been chosen to have a 3-3 architecture. By applying local transformations on its leg endpoint locations, the large family of 6-legged flagged manipulators has been expanded. Then, by replacing 2-leg groups by kinematically equivalent serial chains, the much larger family of 3-legged flagged manipulators has also been derived.

In sum, flagged parallel manipulators have singularity spaces with a well-structured topology, which is the same for all members of this large class, irrespective of changes in their kinematic parameters.

We are currently exploring the possibility of carrying out a similar analysis for the families of manipulators derived from other 3-3 parallel architectures.

## APPENDIX

### A. Stratification of the flag manifold $\mathcal{F}\mathrm{lag}(4)$

Denote by $V_0 \subset V_1 \subset V_2 \subset V_3 = \mathbb{P}^3$ the reference flag. Let $\sum_4$ be set of permutations of $4$ elements, and consider $w \in \sum_4$.

*Definition 3 (Bruhat or Schubert cell):* The Bruhat or Schubert cell $B^w$ associated to the permutation $w$ is the set of all flags whose flag features have incidence relations with the reference flag determined by $w$ in the following way:

$$B^w = \{(V_0^*, V_1^*, V_2^*, V_3^*) \in \mathcal{F}lag(4) : \dim(V_p^* \cap V_q) = r_w(p,q) \text{ for } 1 \le p, q \le 3\}$$

where $r_w(p,q) = \mathrm{card}\{i \le p : w(i) \le q\} - 1$.

It is a classical result that each choice of a reference flag gives a stratification or cell decomposition of the flag manifold:

*Theorem 1 (Stratification of the flag manifold $\mathcal{F}\mathrm{lag}(4)$):* (see [13] Ch. 13, Th. 4.3 or [11] Ch. 10): The disjoint union of all Bruhat cells $B^w$ with $w \in \sum_4$ is a stratification for $\mathcal{F}lag(4)$:

$$\mathcal{F}lag(4) = \cup_{w \in \sum_4} B^w, \tag{4}$$

and $B^u \cap \overline{B^w} \neq \emptyset$ if and only if $B^u \subset \overline{B^w}$.

The structure of each cell and the adjacencies between them are also classically well established:

*Proposition 1:* (see [13] Ch. 13, Prop. 4.7 or [11] Ch. 10, Prop. 7):

1) $B^w$ is isomorphic to the affine space $\mathbb{R}^{\mathrm{length}(w)}$.
2) If $B^w$ and $B^u$ are two cells of consecutive dimensions $\mathrm{length}(w) = \mathrm{length}(u)+1$, then $\overline{B^w} \supset B^u$ if and only if there exists a transposition $t \in \sum_4$ so that $w = tu$.

### B. Stratification of the set of affine flags $\mathcal{F}_{\mathcal{A}}(\mathbb{P}^3)$

Fix from now on an affine reference flag, that is, $V_0 \subset V_1 \subset V_2 \subset V_3 = \mathbb{P}^3$ with $V_0 \notin \Pi_\infty$. Consider the corresponding cell decomposition of $\mathcal{F}lag(4)$ as in (4). When restricted to the open subset of the affine flags $\mathcal{F}_{\mathcal{A}}(\mathbb{P}^3)$ the partition (4) clearly induces a partition:

$$\mathcal{F}_{\mathcal{A}}(\mathbb{P}^3) = \cup_{w \in \sum_4} (B^w \cap \mathcal{F}_{\mathcal{A}}(\mathbb{P}^3)). \tag{5}$$

Since the reference flag is an affine flag, none of the above intersections is empty. However it might happen that some cell $B^w$ would split off into two connected components: indeed, $B^w \cap \mathcal{F}_{\mathcal{A}}(\mathbb{P}^3)$ is a unique connected component if and only if the permutation $w$ starts with $w(1) = 1$. To see this, choose an affine reference frame $\{V_0; \mathbf{e}_1, \ldots, \mathbf{e}_n\}$ attached to the reference flag, namely $\mathbf{e}_1$ is a vector representing the improper point $\mathbf{e}_1^\infty = V_1 \cap H_\infty$, $\mathbf{e}_2$ is a vector representing another point $\mathbf{e}_2^\infty$ on the improper line $V_2 \cap H_\infty$, and so on. Let $(x_1, \ldots, x_n)$ denote the projective coordinates in its associated projective reference $\{V_0, \mathbf{e}_1^\infty, \ldots, \mathbf{e}_n^\infty; \mathbf{a}\}$.

First, let us give a construction of the isomorphism of Proposition 1. Observe that each flag $\mathcal{V}^* = (V_0^*, V_1^*, V_2^*) \in B^w$ is represented by a unique $4 \times 4$ matrix $\mathbf{M}$ whose first three rows span the flag features of $\mathcal{V}^*$, and where the $p$-th row has a $1$ in the $w(p)$-th column, with all $0$'s at the right and below of this $1$. $\mathbf{M}$ will be called the *canonical matrix* representing the flag $\mathcal{V}^*$. For example, for $w = (3,4,2,1)$ the cell $B^w$ is isomorphic to the set of matrices of the form

$$\begin{pmatrix} * & * & 1 & 0 \\ * & * & 0 & 1 \\ * & 1 & 0 & 0 \\ 1 & 0 & 0 & 0 \end{pmatrix},$$

where the stars denote arbitrary real numbers; in this case $B^w$ is the set of all flags whose vertex lies on the plane $V_2 : \{x_4 = 0\}$. The number of stars appearing in the canonical matrices parameterizing the flags of $B^w$ (for an arbitrary $w$) turns out to be the length of $w$ (see [11] 10.2).

If we switch to affine flags and we take up again the example of the permutation $w = (3,4,2,1)$, the affine flags of $B^w$ are the disjoint union of two cells: one of them is isomorphic to the set of matrices of the form

$$\begin{pmatrix} a & * & 1 & 0 \\ * & * & 0 & 1 \\ * & 1 & 0 & 0 \\ 1 & 0 & 0 & 0 \end{pmatrix}, \tag{6}$$

where the stars denote arbitrary real numbers and $a$ denotes a positive real number; the other cell is isomorphic to the set of matrices of the same form (6) where the stars denote arbitrary real numbers and $a$ denotes a negative real number. The matrices of the form (6) where $a$ is zero correspond to flags which are not affine.

For a permutation $w$ with $w(1) > 1$, let $B_+^w$ denote the connected component of $B^w \cap \mathcal{F}_{\mathcal{A}}(\mathbb{P}^3)$ formed from the flags $\{(v^*, l^*, p^*) \in B^w : v^* = (x_1, x_2, x_3, x_4) \text{ with } x_1 x_{w(1)} > 0\}$ and let $B_-^w$ equal $\{(v^*, l^*, p^*) \in B^w : v^* = (x_1, x_2, x_3, x_4) \text{ with } x_1 x_{w(1)} < 0\}$. Observe that the quotient $\frac{x_1}{x_{w(1)}}$ is the $(1,1)$ entry of the canonical matrix of any flag belonging to $B^w$. If $w(1) = 1$, set $B_+^w = B_-^w = B^w$.

The interesting point of partition (5) is that it provides a stratification of $\mathcal{F}_{\mathcal{A}}(\mathbb{P}^3)$ and that the adjacencies between the cells may also be determined:

*Theorem 2:* 1) The partition

$$\mathcal{F}_{\mathcal{A}}(\mathbb{P}^3) = \bigcup_{\substack{w\in\Sigma_4\\ w(1)\neq 1}} (B^w_+ \cup B^w_-) \cup \bigcup_{\substack{w\in\Sigma_4\\ w(1)=1}} B^w \qquad (7)$$

is a stratification for the affine flags.

2) Let $u$ and $w$ be two permutations of $\sum_4$.
   a) If $B^u \subseteq \overline{B^w}$, then $B^u_+ \subseteq \overline{B^w_+}$ and $B^u_- \subseteq \overline{B^w_-}$.
   b) If $B^u \subseteq \overline{B^w}$ and $u(1) < w(1)$, then $B^u_+ \subseteq \overline{B^w_-}$ and $B^u_- \subseteq \overline{B^w_+}$.

   Moreover, there are no other adjacencies between cells than those in the two cases above.

*Proof:* The proof follows after a deeper insight into the canonical matrices associated to the flags; for details see [1]. ■

### C. Stratification of configuration space $\mathbb{R}^3 \times SO(3)$

Via the 4-fold covering morphism $\pi : \mathbb{R}^3 \times \mathrm{SO}(3) \to \mathcal{F}_{\mathcal{A}}(\mathbb{P}^3)$, introduced in Section IV-B, the stratification of $\mathcal{F}_{\mathcal{A}}(\mathbb{P}^3)$ induces a stratification of $\mathbb{R}^3 \times \mathrm{SO}(3)$. We shall focus on the cells of dimensions 5 and 6 and in determining their adjacencies. To this aim we need to introduce some concepts and results on paths and path lifting.

*Definition 4:* A path in a manifold $S$ is a continuous map $\gamma$ from the unit real interval $[0,1]$ to $S$; $\gamma(0)$ and $\gamma(1)$ are called the origin and end, respectively, of $\gamma$; $\gamma$ is also called transition between $\gamma(0)$ and $\gamma(1)$. The path is closed if $\gamma(0) = \gamma(1)$. The inverse path of $\gamma$ is defined as $\gamma^{-1}(t) = \gamma(1-t)$.

Given a covering morphism $\pi : \widetilde{S} \to S$, a lift of the path $\gamma : [0,1] \to S$ is a path on $\widetilde{S}$, $\widetilde{\gamma} : [0,1] \to \widetilde{S}$, so that $\pi \circ \widetilde{\gamma} = \gamma$.

*Theorem 3 (Unicity of the lifting; see [18] 17.6):* Let $\pi : \widetilde{S} \to S$ be a covering morphism. Given a path $\gamma : [0,1] \to S$ and a point $x \in \widetilde{S}$ so that $\pi(x) = \gamma(0)$, there is a unique lift $\widetilde{\gamma}$ of the path $\gamma$ so that $\widetilde{\gamma}(0) = x$.

Recall that to characterize each of the 8 6D cells of $\mathbb{R}^3 \times \mathrm{SO}(3)$ we use the triple of signs corresponding to the orientation of the three tetrahedra appearing in Fig. 5. Observe that the four 6D cells $(\varepsilon,+,+)$, $(\varepsilon,+,-)$, $(\varepsilon,-,+)$ and $(\varepsilon,-,-)$ map by the covering $\pi$ to $B^{(4,3,2,1)}_{\varepsilon}$ for $\varepsilon \in \{+,-\}$.

*Theorem 4:* Each pair of 6D cells of $\mathbb{R}^3 \times \mathrm{SO}(3)$ differing in only one sign are separated by two different 5D cells which are both of type $p - v^*$, $l \cdot l^*$ or $v - p^*$, if the differing sign occupies the first, second or third position, respectively.

*Proof:* Directly due to the 4-fold covering $\pi$, there are two different 5D cells of type $p - v^*$ separating each pair of 6D cells $(+,\varepsilon_1,\varepsilon_2)$ and $(-,\varepsilon_1,\varepsilon_2)$ for any $\varepsilon_1,\varepsilon_2 \in \{+,-\}$. Fix a flag $\mathcal{V}^* = \mathbf{q}(\mathcal{V}) \in B^{(4,3,2,1)}_{\varepsilon}$, with $\varepsilon \in \{+,-\}$. We will consider in $\mathcal{F}_{\mathcal{A}}(\mathbb{P}^3)$ four different paths with origin $\mathcal{V}^*$ that will lie entirely in $B^{(4,3,2,1)}_{\varepsilon}$ except at a point, at which a 5D cell will be crossed. Namely, $\rho_x$ and $\rho_z$ are the rotations from 0 to $\pi$ radians about the $x$-axis and $z$-axis, respectively, of a orthogonal reference frame attached to the flag $\mathcal{V}^*$; $\rho_x^{-1}$ and $\rho_z^{-1}$ are the respective inverse paths, i.e., rotations from 0 to $-\pi$ radians. Observe that the path $\rho_x(t) = (v^*, l^*, p^*(t))$ crosses the 5D cell $(v - p^*)^{\varepsilon}$ at the point $\rho_x(t_0) = (v^*, l^*, p^*(t_0))$ at which the platform plane $p^*(t_0)$ touches the vertex $v$ of the base plane, and that $\rho_z(t) = (v^*, l^*(t), p^*)$ crosses the 5D cell $(l \cdot l^*)^{\varepsilon}$ at the point $\rho_z(t_1) = (v^*, l^*(t_1), p^*)$ at which the platform line $l(t_1)$ goes through the point $p^* \cap l$.

Let $\{\mathbf{q}, \mathbf{R}_x\mathbf{q}, \mathbf{R}_y\mathbf{q}, \mathbf{R}_z\mathbf{q}\}$ be the 4 points in the fiber of $\mathcal{V}^* = \mathbf{q}(\mathcal{V})$. Consider the lifts of the paths $\rho_x$, $\rho_x^{-1}$, $\rho_z$ and $\rho_z^{-1}$ with origin $\mathbf{q}$ (cf. Theorem 3): $\widetilde{\rho_x}$, $\widetilde{\rho_x^{-1}}$, $\widetilde{\rho_z}$ and $\widetilde{\rho_z^{-1}}$. Notice that the transitions $\widetilde{\rho_x}$ and $\widetilde{\rho_x^{-1}}$ do not intersect except at the ends; the different configurations $\mathbf{q}_{t_0}$ and $\mathbf{q}'_{t_0}$ at which $\widetilde{\rho_x}$ and $\widetilde{\rho_x^{-1}}$, respectively, cross a 5D cell share the same flag $\rho_x(t_0)$, that is, $\pi(\mathbf{q}_{t_0}) = \pi(\mathbf{q}'_{t_0}) = \rho_x(t_0)$; at $\mathbf{q}_{t_0}$ and $\mathbf{q}'_{t_0}$ the volume of the last tetrahedra appearing in Fig. 5 becomes zero. Hence each transition crosses a different 5D cell in $\mathbb{R}^3 \times \mathrm{SO}(3)$ of type $v - p^*$ and both transitions join two 6D cells whose differing sign occupies the third position. An analogous reasoning applies for transitions $\widetilde{\rho_z}$ and $\widetilde{\rho_z^{-1}}$: each of them crosses a different 5D cell in $\mathbb{R}^3 \times \mathrm{SO}(3)$ of type $l \cdot l^*$ and both transitions join two 6D cells whose differing sign occupies the second position. Finally a similar reasoning can be carried out with the lifts of the paths $\rho_x$ and $\rho_x^{-1}$ with origin $\mathbf{R}_z\mathbf{q}$, and with the lifts of the paths $\rho_z$ and $\rho_z^{-1}$ with origin $\mathbf{R}_x\mathbf{q}$ proving, thus completely, the statement of the Theorem and the adjacencies displayed in Fig. 16. ■

## REFERENCES


[1] M. Alberich-Carramiñana, V. González, and C. Torras, "The topology of singularities of flagged parallel manipulators," *IRI Technical Report*, 2005 (available at http://www-iri.upc.es/people/torras/articles/IRIRep05.pdf).

[2] P. Ben-Horin and M. Shoham, "Singularity condition of six degree-of-freedom three-legged parallel robots based on Grassmann-Caley algebra," *IEEE Trans. on Robotics*, to appear.

[3] I.A. Bonev and C.M. Gosselin, "Singularity Loci of Planar Parallel Manipulators with Revolute Joints," 2nd Workshop on Computational Kinematics, Seoul, Korea, pp. 291-299, 2001.

[4] H. Bruyninckx, "Closed-form forward position kinematics for a (3-1-1-1)$^2$ fully parallel manipulator," *IEEE Trans. on Robotics and Automation*, Vol. 14, No. 2, pp. 326-328, 1998.

[5] H. Bruyninckx, "Forward kinematics for Hunt-Primrose parallel manipulators," *Mechanism and Machine Theory*, Vol. 34, pp. 657-664, 1999.

[6] C.L. Collins and G.L. Long, "The Singularity Analysis of an In-Parallel Hand Controller for Force-Reflected Teleoperation," *IEEE Trans. on Robotics and Automation*, Vol. 11, No. 5, pp. 661-669, 1995.

[7] C.L. Collins and J.M. McCarthy, "The singularity loci of two triangular parallel manipulators," Proc. of the *IEEE Int. Conf. on Advanced Robotics*, pp. 473-479, 1997.

[8] R. DiGregorio, "Analytic formulation of the 6-3 fully-parallel manipulator's singularity determination," *Robotica*, Vol. 19, pp. 663-667, 2001.

[9] R. DiGregorio, "Singularity-locus expression of a class of parallel mechanism," *Robotica*, Vol. 20, pp. 323-328, 2002.

[10] D.M. Downing, A.E. Samuel, and K.H. Hunt, "Identification of the special configurations of the octahedral manipulator using the pure condition," *The International Journal of Robotics Research*, Vol. 21, No. 2, pp. 147-160, 2002.

[11] W. Fulton, *Young Tableaux*, London Mathematical Society Student Texts, 35. Cambridge University Press, 1997.

[12] C. Gosselin and J. Angeles, "Singularity Analysis of Closed-Loop Kinematic Chains," *IEEE Trans. on Robotics and Automation*, Vol. 6, No. 3, pp. 281-290, 1990.

[13] H. Hiller, *Geometry of Coxeter Grups*, Research Notes in Mathematics, Pitman Books, London, 1982.

[14] Z. Huang, L.H. Chen, and Y.W. Li, "The singularity principle and property of Stewart parallel manipulator," *Journal of Robotic Systems*, Vol. 20, No. 4, pp. 163-176, 2003.

[15] K.H. Hunt and E.J.F. Primrose, "Assembly configurations of some in-parallel-actuated manipulators," *Mechanism and Machine Theory*, Vol. 28, No. 1, pp. 31-42, 1993.

[16] C. Innocenti and V. Parenti-Castelli, "Singularity-free evolution from one configuration to another in serial and fully-parallel manipulators," *ASME* $22^{nd}$ *Biennial Mechanisms Conference: Robotics, Spatial Mechanisms, and Mechanical Systems*, Vol. 45, pp. 553-560, 1992.
[17] D. Kim, and W.Y. Chung, "Analytic singularity equation and analysis of six-dof parallel manipulators using local structuration method," *IEEE Trans. on Robotics and Automation*, Vol. 5, No. 4, pp. 612-622, 1999.
[18] C. Kosniowski, *A First Course in Algebraic Topology*, Cambridge University Press, 1980.
[19] H. Li, C.M. Gosselin, M.J. Richard, and B.M. St-Onge, "Analytic form of the six-dimensional singularity locus of the general Gough-Stewart platform," *Journal of Mechanical Design*, Vol. 128, No. 1, pp. 279-287, 2006.
[20] J.-P. Merlet, *Parallel Robots*, Springer, 2000.
[21] A.S. Posamenteier and C.T. Salkind, *Challenging Problems in Geometry*, The MacMillan Company, New York, 1970.
[22] P. Sankaran and P. Zvengrowski, "Stable parallelizability of partially oriented flag manifolds II," *Can. J. Math*, Vol. 49, No. 6, pp. 1323-1339, 1997.
[23] S.-K. Song and D.-S. Kwon, "A tetrahedron approach for a unique closed-form solution of the forward kinematics of six-dof parallel mechanisms with multiconnected joints," *Journal of Robotic Systems*, Vo. 19, No. 6, pp. 269-281, 2002.
[24] B.M. St-Onge, C.M. Gosselin, "Singularity analysis and representation of the general Gough-Stewart platform," *Int. J. Robotics Research*, Vol. 19, No. 3, pp. 271-288, 2000.
[25] C. Torras, F. Thomas, M. Alberich-Carramiñana, "Stratifying the singularity loci of a class of parallel manipulators," *IEEE Trans. on Robotics*, Vol. 22, No. 1, pp. 23-32, 2006.
[26] A. Wolf and M. Shoham, "Investigation of parallel manipulators using linear complex approximation," *Trans. of the ASME, Journal of Mechanical Design*, Vol. 125, pp. 565-
[27] Ch. Zhang and S-M. Song, "Forward kinematics of a class of parallel (Stewart) platforms with closed-form solutions", *Proc. of the Int. Conf. on Robotics and Automation*, pp. 2676-2681, 1991.